nature geoscience

SUPPLEMENTARY INFORMATION

DOI: 10.1038/NGEO1642

Supplementary Material for *Summertime Climate Response to a Mountain Pine Beetle Disturbance in British Columbia*

Assessment of MODIS Data Quality

Several techniques are applied to investigate MODIS data quality prior to analysis of the multi-pixel averages presented in Figures 2, 4, and S3. First, visual inspection of the individual time series suggests that interannual variations between pixels are strongly correlated, indicating that large-scale climatic variations exceed the statistical fluctuations expected from measurement uncertainty. Examination of the MODIS quality flags available for daytime and nighttime temperature lends further evidence to this hypothesis. For example, while the reported uncertainty for the 8-day daytime temperature measurements is $< 1^\circ$, the typical interseasonal variation is much larger, with a mean value of 4.2°.

Data quality flags are not included in the the MODIS broadband albedo and monthly evapotranspiration products. To systematically examine the statistical properties of all three products, we therefore construct power spectra for the individual pixels. The average power spectrum for each variable analyzed is shown in Figure S1, which demonstrates that all three variables considered are of relatively high quality. The noisiest is $T_{11} - T_{21}$, which implies signal-to-noise ratios on seasonal timescales of $\gtrsim 10$. This analysis confirms that the variability of the observed summertime data is primarily physical in origin.

The analysis described here considers statistical errors only, neglecting potential systematic effects. Systematic errors are diagnosed in the results section of the main text, through the consistency checks provided by the water and energy balance analyses, and the comparison to precipitation and sapflow measurements.

Simple Model for Canopy Evapotranspiration

To help validate the MODIS evapotranspiration data pre- and post-disturbance, we require a simple functional form for evapotranspiration that describes its dependence on pre-disturbance forest surface density and the fraction of remaining live trees post-disturbance. Total evapotranspiration for a forest canopy can be idealized as the sum of living tree transpiration and evaporation from soil and vegetation:

$$E = E_{\mathrm{live}} + E_{\mathrm{evap}}. \tag{1}$$

Total net radiation to the tree-soil surface is divided between the soil, the living tree canopy, and the dead tree canopy:

$$R_N = R_{N,\,\mathrm{soil}} + R_{N,\,\mathrm{live}} + R_{N,\,\mathrm{dead}}. \tag{2}$$

The radiation incident on the soil surface depends on the level of extinction by overlying living and dead trees[†] and is thus assumed to be governed by a Beer-Lambert law:

$$R_{N,\,\mathrm{soil}} = R_N e^{-\Sigma_0/\Sigma_{\mathrm{crown}}}. \tag{3}$$

[†]Based on the observation that beetle-killed trees begin to lose their needles 2-4 years following attack [1] and the majority of mortality was 2005-2006, we assume dead trees are just as capable of shading the ground and adjacent trees as their living counterparts.

Here, Σ_0 is the forest surface density pre-disturbance and Σ_{crown} is the surface density at which the optical depth to the forest floor in the direction of incoming radiation is unity. Combining equations 2 and 3 yields

$$R_{N,\,\mathrm{live}} + R_{N,\,\mathrm{dead}} = R_N(1 - e^{-\Sigma_0/\Sigma_{\mathrm{crown}}}). \tag{4}$$

Defining f_{live} as the number of living trees post-disturbance relative to the total,

$$f_{\mathrm{live}} = \frac{R_{N,\,\mathrm{live}}}{R_{N,\,\mathrm{live}} + R_{N,\,\mathrm{dead}}}. \tag{5}$$

Therefore, the net radiation to the living trees increases with forest surface density as

$$R_{N,\,\mathrm{live}} = f_{\mathrm{live}} R_N(1 - e^{-\Sigma_0/\Sigma_{\mathrm{crown}}}). \tag{6}$$

In the case that trees have plentiful water, transpiration scales approximately in proportion to net radiation[2] such that

$$E_{\mathrm{live}} = E_{\mathrm{canopy,\,max}} f_{\mathrm{live}}(1 - e^{-\Sigma_0/\Sigma_{\mathrm{crown}}}), \tag{7}$$

where $E_{\mathrm{canopy,\,max}}$ is the maximum canopy transpiration corresponding to a fully live canopy and a fully shaded soil surface. The full model for forest evapotranspiration is then written as

$$E = E_{\mathrm{canopy,\,max}} f_{\mathrm{live}}(1 - e^{-\Sigma_0/\Sigma_{\mathrm{crown}}}) + E_{\mathrm{evap}}. \tag{8}$$

Estimate of Forest Surface Density for a Fully Shaded Soil Surface

The forest volume surface density at which the optical depth at the forest floor is unity is

$$\Sigma_{\mathrm{crown}} = \frac{V_{1\mathrm{tree}}}{d^2_{\mathrm{crown}}}, \tag{9}$$

where $V_{1\mathrm{tree}}$ is the typical tree volume and d_{crown} is the characteristic tree spacing.

From the standpoint of tree physiology, we expect the maximum optical depth in the direction of the Sun through a single tree to be of order unity. In this case, all light travels through approximately one tree (see Figure S2). The characteristic tree spacing at which the optical depth at the forest floor is unity is therefore

$$d_{\mathrm{crown}} \sim \frac{h_{\mathrm{crown}}}{2f \tan\theta}, \tag{10}$$

where h_{crown} is the typical crown height and θ is the characteristic solar elevation at which evaporation takes place. The factor f depends on how the trees are spaced in two dimensions. For hexagonal close packing and a stationary Sun, $f = 1$; in the case that the tree crowns are infinitely thin, $f = 2$. Lodgepole pine crowns are much taller than they are wide[3], and we therefore adopt $f = 2$.

Combining equations 9 and 10, the volumetric forest surface density corresponding to d_{crown} is then

$$\Sigma_{\mathrm{crown}} \sim 16\, V_{1\mathrm{tree}} \frac{\tan^2\theta}{h_{\mathrm{crown}}^2}. \tag{11}$$

The maximum solar elevation on the summer solstice at 55°N is $90^\circ - (55^\circ - 23.5^\circ) = 58.5^\circ$. We take θ as half this value ($\theta \sim 30^\circ$), or approximately the mean daytime solar elevation in summer. Adopting a typical tree volume, height, and crown-to-height ratio of $V_{1\mathrm{tree}} = 0.25\,\mathrm{m}^3$, $h_{\mathrm{tree}} = 25\,\mathrm{m}$, and $f_{\mathrm{crown}} = 0.4$, respectively[3,4], the expected forest density at which shading

becomes significant is approximately:

$$\Sigma_{\mathrm{crown}} \sim 13,000\,\mathrm{m}^3\,\mathrm{km}^{-2}\,\frac{V_{1\mathrm{tree}}}{0.25\,\mathrm{m}^3}\left(\frac{\tan\,\theta}{\tan 30^\circ}\right)^2\left(\frac{25\,\mathrm{m}}{h_{\mathrm{tree}}}\right)^2\left(\frac{0.4}{f_{\mathrm{crown}}}\right)^2, \quad (12)$$

in good agreement with the value of Σ_{crown} fitted to the MODIS data (see main text, *Stand-level sapflow measurements support MODIS transpiration*).

Albedo Changes Post-Disturbance

Figure S3 shows the analog to Figure 2 for MODIS albedo, demonstrating that changes to albedo are small ($\lesssim 1\%$) for all surface densities and levels of mortality. The suggested change to the absorbed shortwave flux at the surface is $\Delta AS_{\downarrow} \lesssim 2\,\mathrm{W\,m}^{-2}$, which is small in comparison to observed changes in evapotranspiration ($\Delta\lambda E \lesssim 30\,\mathrm{W\,m}^{-2}$, Figure 4). Thus, we may neglect changes to the surface energy balance resulting from albedo changes.

Relationship between Changes in Evapotranspiration and Changes in Surface Temperature

For a land surface that radiates as a blackbody, the energy balance at the surface is[5]

$$(1-A)S_{\downarrow} + L_{\downarrow} = \lambda E + R + H + G. \quad (13)$$

Here, $S_{\downarrow}$ and $L_{\downarrow}$ are the incident shortwave and longwave radiative fluxes, respectively, and A is the albedo. The mass flux of evaporated water is E and λ is the latent heat of vaporization per unit mass, such that λE is the latent heat flux to the atmosphere. The radiative and sensible heat fluxes to the atmosphere are R and H, respectively, and G is the conductive flux into the surface. The

change to the surface energy balance post-disturbance, denoted by Δ, is obtained by differentiating equation 13. If the disturbance does not change the incoming radiative fluxes,

$$-\Delta(AS_{\downarrow}) \simeq \Delta(\lambda E) + \Delta R + \Delta H + \Delta G. \tag{14}$$

The equilibrium conductive flux in forested areas is generally small compared to the other terms ($\lesssim 10\%$ of the net radiation[6]), such that to first order, we expect $\Delta G \approx 0$:

$$-\Delta(AS_{\downarrow}) \simeq \Delta(\lambda E) + \Delta R + \Delta H. \tag{15}$$

The previous section showed that changes in the absorbed shortwave flux are small compared to changes in the latent heat flux, allowing equation 15 to be yet further simplified:

$$\Delta(\lambda E) \simeq -(\Delta R + \Delta H). \tag{16}$$

Thus, changes to the latent heat flux are fully compensated by changes to the sum of the outgoing radiative and convective heat fluxes. The outgoing radiative flux is governed simply by the Stefan-Boltzmann law,

$$R = \sigma(T_s + 273.15)^4, \tag{17}$$

where σ is the Stefan-Boltzmann constant ($5.67 \times 10^{-8}\,\mathrm{W\,m^{-2}\,K^{-4}}$) and T_s is the surface temperature ($^{\circ}\mathrm{C}$). In a bulk formulation, the sensible heat flux is[7]

$$H = -\rho C_p \frac{T_a - T_s}{r_a}, \tag{18}$$

where ρ is the density of air ($\mathrm{kg\,m^{-3}}$), $C_p = 1005\,\mathrm{J\,kg^{-1}\,K^{-1}}$ is the heat capacity of air, r_a is the aerodynamic resistance to heat transfer ($\mathrm{s\,m^{-1}}$), and T_a is the air temperature ($^{\circ}\mathrm{C}$). In coniferous

forests, air temperature varies approximately linearly with surface temperature ($T_a \simeq mT_s$)[8], such that

$$H \simeq \rho C_p \frac{(1-m)\,T_s}{r_a}. \tag{19}$$

Differentiating equations 17 and 19, equation 16 becomes

$$\Delta(\lambda E) \simeq -\left(4\sigma(T_s + 273.15)^3 + \frac{\rho C_p}{r_a}(1-m)\right)\Delta T_s. \tag{20}$$

This equation can be written in terms of observables using the conversion factors, $c_E \equiv \Delta(\lambda E)/\Delta E$ and $c_T \equiv \Delta T_s/\Delta(T_{11} - T_{21})$, derived in the next section:

$$\Delta E \simeq -\frac{c_T}{c_E}\left(4\sigma(T_s + 273.15)^3 + \frac{\rho C_p}{r_a}(1-m)\right)\Delta(T_{11} - T_{21}). \tag{21}$$

In the main text, we use equation 20 together with the typical stand temperature and the linear least squares slope of ΔT_s versus $\Delta(\lambda E)$ to estimate the sensible heat flux sensitivity, $\rho C_p(1-m)/r_a$, to a given change in temperature, ΔT_s. This technique may slightly overestimate the convective sensitivity, as even in this linear approximation, we more precisely derive the sum of the convective and conductive sensitivities. However, as discussed above, previous measurements in forested areas suggest that post-disturbance changes in G are likely to be small. Furthermore, the convective sensitivity we derive is in good agreement with that expected from measurements at typical coniferous forest flux tower sites, giving us additional confidence that changes in G are indeed small.

We note that previous work has also shown that post-disturbance, decreases in winter and spring surface temperatures may occur[9], which could potentially result in modest decreases in

summertime soil temperatures. In equilibrium, the conductive flux is parameterized as

$$G = k\frac{T_s - T_g}{\Delta z}, \tag{22}$$

where T_g is the soil temperature at depth Δz, and k is the thermal conductivity. Thus, in addition to post-disturbance changes in T_s, large changes in T_g (or k) could in principle lead to observable changes in G. We see no evidence for significant departures from linearity in our plot of ΔT_s versus $\Delta(\lambda E)$ (Figure 4d). Therefore in this first study, we are able to explain present observations without requiring changes in these variables. Further investigating the interplay between seasons and potential departures from linearity will be a topic for future work.

Temperature and Evapotranspiration Conversion Factors

The conversion between evapotranspiration and latent heat flux simply requires multiplication by the latent heat of vaporization, which varies only modestly over the range of observed temperatures. Adopting a typical temperature of $12\,^{\circ}\mathrm{C}$, $c_E \equiv \Delta(\lambda E)/\Delta E = 0.93\,\mathrm{W\,m^{-2}/(mm\,mon^{-1})}$. The second conversion between the change in the day-night temperature difference and the change in mean surface temperature requires assumptions about the diurnal temperature cycle. We adopt a sinusoidal variation, consistent with mid-summer station measurements[10],

$$T(t) = \frac{T_{\mathrm{Max}} - T_{\mathrm{Min}}}{2}\sin(\omega t) + \frac{T_{\mathrm{Max}} + T_{\mathrm{Min}}}{2}. \tag{23}$$

Here, T_{Max} and T_{Min} are the daily maximum and minimum temperatures, respectively, and $\omega = 2\pi/24\,\mathrm{hr}$. Nighttime latent heat fluxes are small, such that we expect the minimum temperature

change post-disturbance is negligible[11,12]:

$$\Delta T(t) \simeq \frac{\Delta T_{\mathrm{Max}}}{2} \sin(\omega t) + \frac{\Delta T_{\mathrm{Max}}}{2}. \tag{24}$$

Employing equation 24 at the times of the MODIS day- and night-time observations (t_{11} and t_{21}),

$$\Delta T_{11} - \Delta T_{21} \simeq \frac{\Delta T_{\mathrm{Max}}}{2} \left[\sin(\omega t_{11}) - \sin(\omega t_{21})\right]. \tag{25}$$

The mean daytime temperature is $T_s = (T_{\mathrm{Max}} + T_{\mathrm{Min}})/2$ such that $\Delta T_s = \Delta T_{\mathrm{Max}}/2$. Rearranging equation 25 yields

$$\frac{\Delta(T_{11} - T_{21})}{\Delta T_s} \simeq \sin(\omega t_{11}) - \sin(\omega t_{21}). \tag{26}$$

Defining the hourly differences between the daily maximum temperature and the measured daytime and nighttime temperatures as $\delta t_{\mathrm{Max,Day}} \equiv t_{11} - t(T_{\mathrm{Max}})$ and $\delta t_{\mathrm{Max,Night}} \equiv t_{21} - t(T_{\mathrm{Max}})$,

$$\Delta T_s \simeq \frac{\Delta(T_{11} - T_{21})}{\cos(\omega\, \delta\, t_{\mathrm{Max,Day}}) - \cos(\omega\, \delta\, t_{\mathrm{Max,Night}})} \equiv c_T \Delta(T_{11} - T_{21}). \tag{27}$$

Station measurements suggest daily peak temperatures at 14:00 local solar time[10], whereas the MODIS observation times are approximately 11:30 and 21:30. Thus, $\delta t_{\mathrm{Max,Day}} = -2.5\,\mathrm{hr}$ and $\delta t_{\mathrm{Max,Night}} = 7.5\,\mathrm{hr}$ such that $c_T = 0.85$.

From equation 23, the average surface temperature is

$$T_s = \frac{T_{11} + T_{21}}{2} - \frac{T_{11} - T_{21}}{2} \frac{\cos(\omega\, \delta\, t_{\mathrm{Max,Day}}) + \cos(\omega\, \delta\, t_{\mathrm{Max,Night}})}{\cos(\omega\, \delta\, t_{\mathrm{Max,Day}}) - \cos(\omega\, \delta\, t_{\mathrm{Max,Night}})}, \tag{28}$$

which evaluates to $11.5\,^{\circ}\mathrm{C}$, averaged over all affected stands in all years considered. The standard deviation in this value is $2.5\,^{\circ}\mathrm{C}$.

#1 Schmid, J. *Net precipitation within small group infestations of the mountain pine beetle*, vol. 508 (USDA Forest Service, Rocky Mountain Forest and Range Experiment Station, 1991).

#2 Priestley, C. & Taylor, R. On the assessment of surface heat flux and evaporation using large-scale parameters. *Monthly Weather Review* **100**, 81–92 (1972).

#3 Sullivan, T., Sullivan, D., Lindgren, P. & Ransome, D. Long-term responses of ecosystem components to stand thinning in young lodgepole pine forest: III. Growth of crop trees and coniferous stand structure. *Forest Ecology and Management* **228**, 69–81 (2006).

#4 Harris, J., Centre, P. F. R., Dawson, A. & Brown, R. *Evaluation of mountain pine beetle damage using aerial photography: Flathead River, B.C., 1980*. Information report (Canadian Forestry Service, 1982).

#5 Bonan, G. *Ecological climatology: concepts and applications* (Cambridge, 2002).

#6 Kustas, W., Daughtry, C. & Van Oevelen, P. Analytical treatment of the relationships between soil heat flux/net radiation ratio and vegetation indices. *Remote Sensing of environment* **46**, 319–330 (1993).

#7 Monteith, J. Evaporation and environment. In *Symposium of the Society for Experimental Biology*, vol. 19, 205–234 (1965).

#8 Wilson, K. *et al*. Energy partitioning between latent and sensible heat flux during the warm season at FLUXNET sites. *Water Resour. Res* **38**, 1294 (2002).

#9 Boon, S. Snow ablation energy balance in a dead forest stand. *Hydrological Processes* **23**, 2600–2610 (2009).

#10 Environment Canada. *National climate data and information archive: Prince George, Smithers, and Quesnel meteorological stations*. (2007).

#11 Vinukollu, R., Wood, E., Ferguson, C. & Fisher, J. Global estimates of evapotranspiration for climate studies using multi-sensor remote sensing data: Evaluation of three process-based approaches. *Remote Sensing of Environment* **115**, 801–823 (2011).

#12 Wiedinmyer, C., Barlage, M., Tewari, M. & Chen, F. Meteorological impacts of forest mortality due to insect infestation in colorado. *Earth Interactions* **16**, 1–11 (2012).

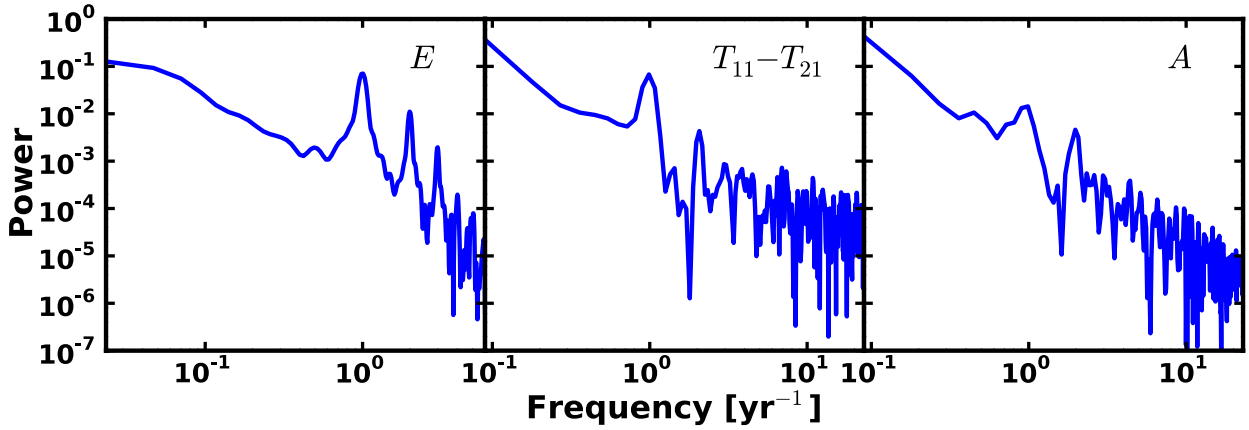

Figure S1 Normalized average power spectra for MODIS evapotranspiration (left), observed day-night temperature difference (middle), and shortwave albedo (right). Prior to computation of the power spectra, all time series were first apodized with a Hanning window function to minimize spectral leakage. Peaks at a frequency of 1 yr^{-1} correspond to the annual cycle; higher frequency peaks represent harmonics. The redness of the spectra for all three variables suggests high signal-to-noise on seasonal timescales.

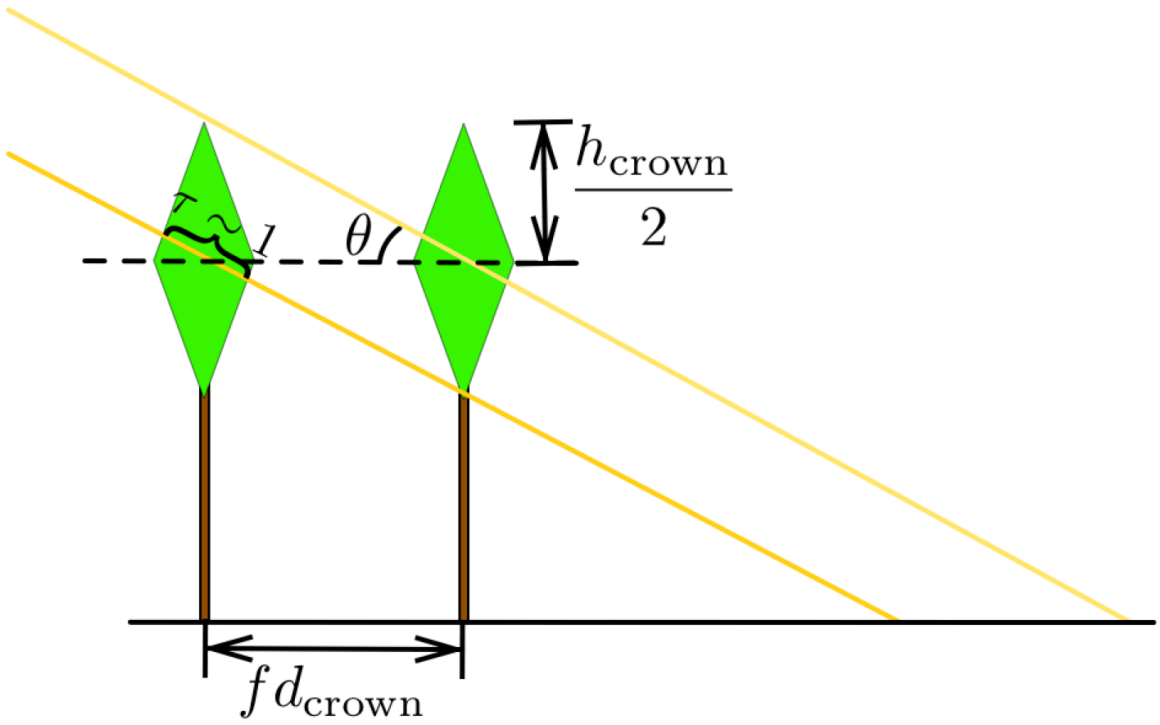

Figure S2 Geometry used in deriving equation 10.

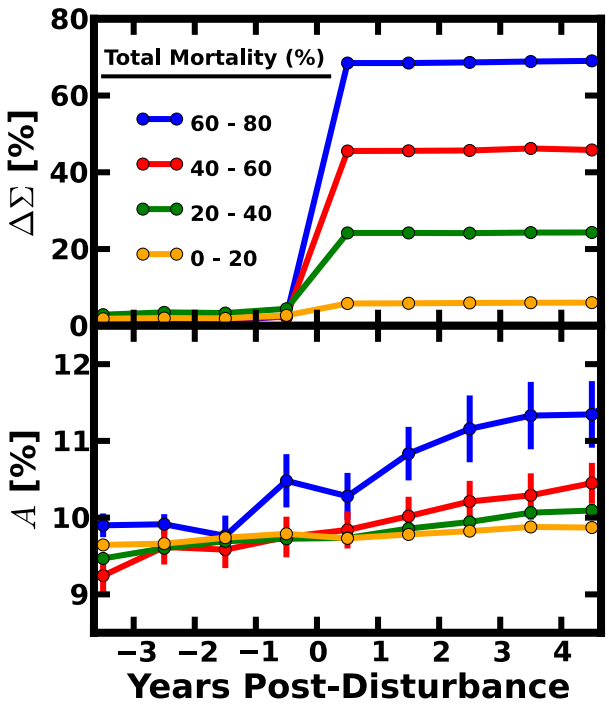

Figure S3 MODIS albedo, A, binned in terms of Σ_0 and $f_{\rm live}$. Changes to albedo are $\lesssim$ 1% for all levels of mortality, suggesting minimal impact on the surface energy balance.